The energetics of steady state heterogeneous shear in mylonitic rock

Mark R. Handy
Geologisches Institut, Universität Bern, Bern (Switzerland)

Abstract

Deformation of Earth's lithosphere below about 5–10 km depth is accommodated heterogeneously in mylonitic shear zones. The persistance of heterogeneous mylonitic deformation to very high strains is a manifestation either of slow transient rheological instability or of heterogeneous steady state creep. The latter possibility may be explained with the following hypothesis: rock deforms at heterogeneous steady state when it acquires a structure that minimizes the overall rate of strain energy dissipation, and when the effective (*i.e.* volume-weighted) rate of strain energy dissipated within this structure is uniform and constant. Thus small volumes of weak anastomozing shear zone deforming at high strain rate dissipate the same amount of viscous strain energy per unit time as do much larger volumes of strong country rock deforming at lower strain rate. The relative magnitude of differential creep stresses in the shear zone and country rock during heterogeneous shear depends on the relative creep parameters of weak and strong rock. Strain localization leads to a modest reduction in the bulk strength of the whole rock at steady state.

1. Introduction

Rock deforms heterogeneously on all scales of observation, from the scale of individual grains and minerals to the scale of Earth's lithosphere. This strain heterogeneity reflects rheological contrasts amongst rocks and minerals that either were inherited from earlier geological events (*e.g.* differences in composition due to metamorphism and magmatism) (Figs. 1(a) and 1(b)) or developed from mechanical instabilities during deformation (*e.g.* shear zones or shear bands) (Figs. 1(c) and 1(d)) [2, 3]. Shear zones are a particularly important type of mechanical heterogeneity because they accommodate relative plate movement and effect the burial and uplift of large volumes of crustal material at plate boundaries (Fig. 2). Earth's lithosphere is therefore a composite material whose constituent phases undergo geometric and rheological changes in time and space.

Shear zones are narrow anastomozing domains of highly strained rock that envelop lozenges of less deformed, or undeformed, country rock (Fig. 2 and 3(a)). The sheared rock is a "mylonite" or is termed "mylonitic" if most of the strain in the rock was accommodated within mineral(s) deforming by thermally activated viscous creep mechanisms (dislocation glide and creep, diffusion- or dislocation-accommodated grain boundary sliding). Often, but not always, mylonitization involves a reduction of grain size in the shear zone with respect to that of the country rock, or protolith. Mylonitization is typical of deformation at depths below 5–10 km where homologous temperatures and effective pressures are sufficiently high ($T_h \geq 0.3$, $P_e \geq 150$ MPa) to favour creep (Fig. 2) [4]. ~~Beyond~~ Above this depth range, the deformation in shear zones involves predominantly brittle fracture and frictional sliding along discrete surfaces, or faults, and is termed "cataclastic" (Fig. 2). The interested reader is referred to reviews by White *et al.* [5], Tullis *et al.* [6], Knipe [7] and Schmid and Handy [8] for discussions of deformation mechanisms and nomenclature in fault rocks.

Mylonitic shear zones occur on scales ranging from kilometre-wide to micrometre-wide zones (see refs. 9 and 10 for some examples). Finite shear strain γ typically increases from the margins to the centres of such shear zones (Fig. 3(b)) [11] and attains values as great as 10–100 [12]. Where it can be established that the shear zone formed during a single continuous kinematic event, strain profiles like that in Fig. 3(b) indicate that strain rate increased into the active shear zone. Consequently, the rock is inferred to have softened locally (*i.e.* becomes less flow resistant) (Fig. 3(c)) with respect to the adjacent country rock (*e.g.* see ref. 13). Although shear zones occupy only a volumetrically small portion of rock on any of these scales, the fact that they are weaker than their host rock suggests that they strongly affect the bulk rheology of Earth's lithosphere [14].

Geological evidence of structural and rheological heterogeneity at high strains leaves earth scientists facing a basic dilemma: is heterogeneous strain an indication of transient rheological behaviour or of steady state? In the former case, heterogeneous shear is regarded only as a stage in the long slow evolution

0921-5093/94/$7.00
SSDI 0921-5093(93)03524-E

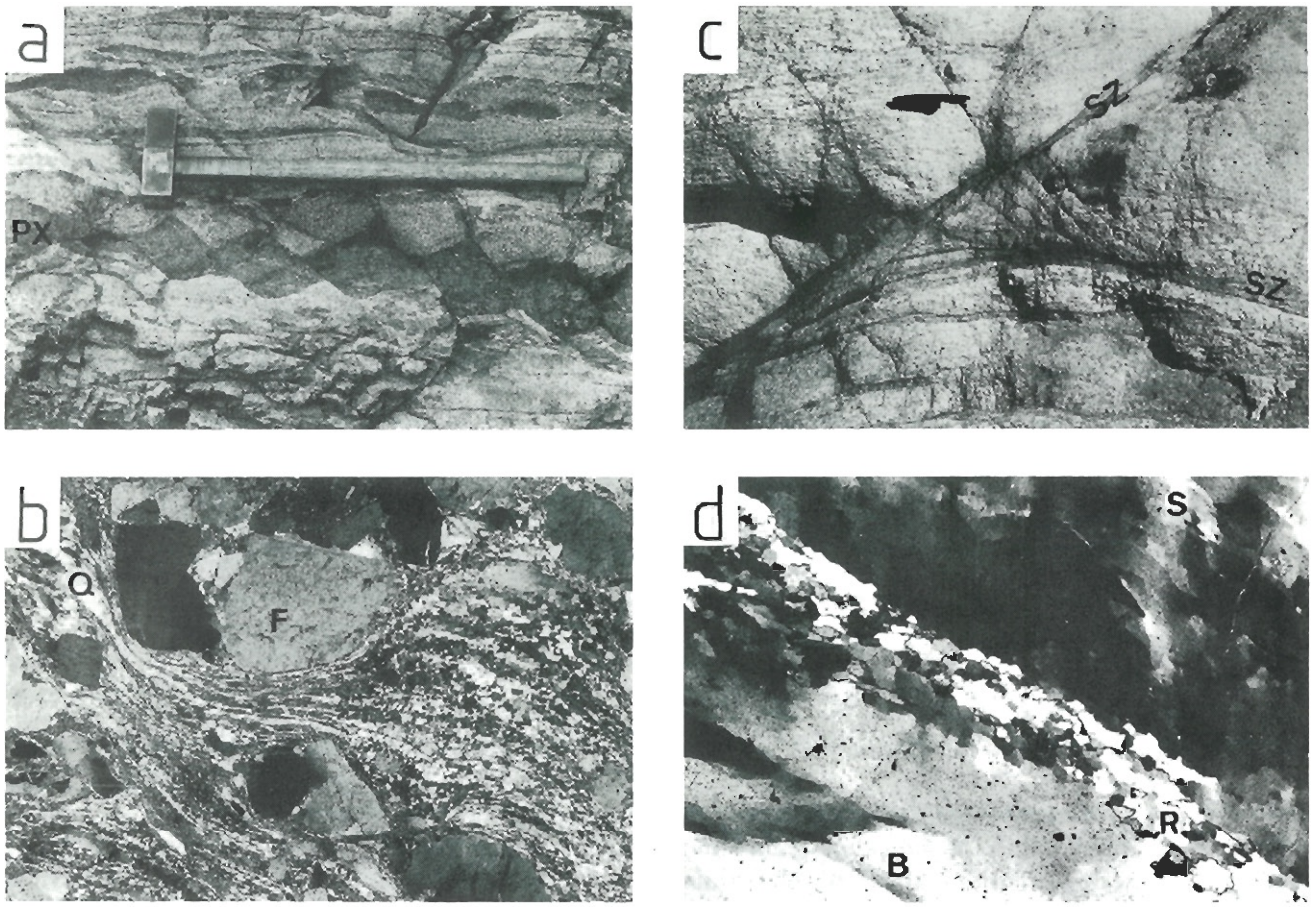

Fig. 1. Some natural examples of heterogeneous mylonitic shear. (a) Lenticular dark layers (boudins) of pyroxene (labelled PX) are deformed within a mylonitic gabbro rock comprising mainly plagioclase feldspar (Ca–Na–Al framework silicate) and pyroxene (Mg–Fe chain silicate). This rock originated at a depth of 20–25 km in Earth's lower crust and was subsequently deformed at a pressure of about 800 MPa and temperature of 700–800 °C [1]. The asymmetrical orientation of the pyroxene segments (below the hammer) reflects rotational mylonitic flow in the gabbro. The hammer (for scale) is 55 cm long. (b) Thin section (30 μm) of mylonitic granite comprising a fine-grained matrix of dynamically recrystallized quartz (Q) and large darker grains of feldspar (F). Grain size refinement in feldspar involves fracturing (top centre) as well as limited dynamic recrystallization and pressure solution at grain rims. Note the localized reduction in size of dynamically recrystallized quartz grains between impinging feldspar grains. This is a thin section viewed in polarized transmitted light. The frame length scales to 5.6 mm. (c) Confluence of two conjugate mylonitic shear zones (SZ) in a mylonitic granite (see the overall configuration in Fig. 3(a)). This rock deformed at a depth of about 10 km and temperature of 300–400 °C [1]. The pen cap (for scale) is 6 cm long. (d) Narrow shear band of fine dynamically recrystallized quartz (R) separating two large elongated grains of unrecrystallized quartz. Note the evidence of dynamic recovery (polygonal subgrains (S) and deformation bands (B)) in the unrecrystallized grains. This is a thin section viewed in polarized transmitted light. The frame length scales to 1.4 mm.

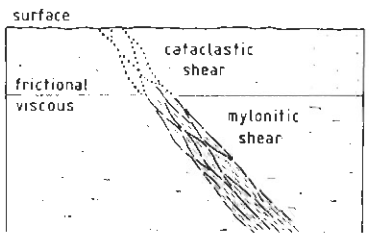

Fig. 2. Schematic profile through the upper to the intermediate part of Earth's lithosphere showing the anatomy of a fault zone. Shallow deformation (less than 5–10 km) is cataclastic and depends strongly on effective pressure, whereas deeper deformation is predominantly mylonitic and depends strongly on temperature and strain rate (see text).

toward homogeneous steady state shear on all scales. However, if rocks can deform heterogeneously at steady state, then criteria are required to explain how and why this occurs on any given scale. To this end, the notion of heterogeneous steady state is accepted here as a working hypothesis.

This paper presents a model of shear zone evolution in which heterogeneously deforming rock is treated as an isothermal system comprising two phases with variable volume proportions and structure. Hypothetical criteria of strain energy rate partitioning are proposed to describe structural and mechanical steady state in

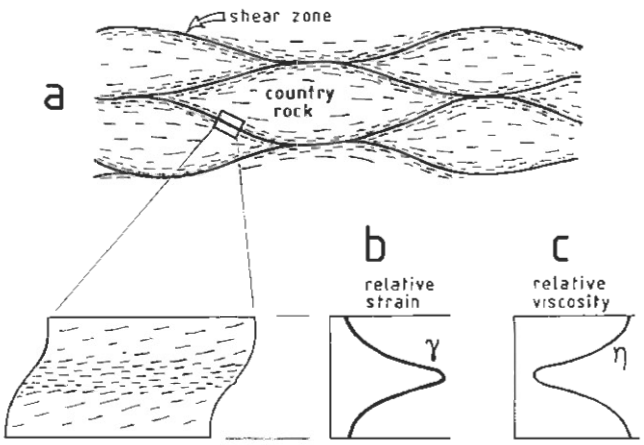

Fig. 3. (a) Anastomozing shear zones in heterogeneously sheared mylonitic rock: – – –, orientation and relative intensity of foliation. (b), (c) Schematic profiles, respectively, of relative shear strain and inferred relative shear viscosity across the shear zone segment outlined in (a).

heterogeneously creeping rock. It is argued that the persistence of heterogeneous deformation to high strains may actually reflect the tendency for mylonitic rock to develop a uniform power dissipation capacity. The criteria of strain energy rate partitioning are then used to show how power dissipation and stress may evolve in heterogeneously deforming rock.

2. A hypothesis of heterogeneous steady state creep

2.1. Boundary conditions and assumptions

In modelling composite materials, it is important to distinguish between the behaviour of the deformational system as a whole (in this case, a rock) and that of its constituent mechanical phases. In this paper, "phase" is defined in a purely mechanical sense as a material with distinctive rheological properties, irrespective of its composition. The adjectives "weak" and "strong" describe the relative strength of two phases as measured at a reference temperature and strain rate outside of the rock. The ratio of these strengths, *i.e.* the "strength contrast" or "competence contrast", is therefore an absolute measure of the relative deformability of the two phases at a given temperature and strain rate.

Consider a monomineralic rock undergoing plane-strain simple shear at constant bulk strain rate $\dot{\gamma}_r$. The rock comprises two mechanical phases, a weak phase (highly sheared rock) and a strong phase (unsheared or less sheared country rock). Both phases are isotropic and deform isochorically, isothermally and compatibly in the solid state by viscous creep. The isothermal condition ensures that there is no localized shear heating and that there are no contributions to the energy and volume budgets in eqns. (4) and (8) below from syntectonic metamorphic reactions or other sources besides the viscous creep of the two phases constituting the rock. This is justified by many microstructural and mineralogical studies on mylonites indicating that the effect of shear heating on localization is minor compared with externally imposed changes in the ambient temperature, pressure and fluid composition [1]. Any dilatancy within, or mass transfer between, the phases is assumed to be negligible. The phase boundaries are ideal discrete surfaces that are incoherent and mobile, *i.e.* they accommodate slip to maintain compatibility and also move laterally as the rheologies and volume proportions of the phases change with strain.

2.2. Geometry and rheology of the phases during shear zone development

The formation of mylonitic shear zones can be divided into two stages, each corresponding to an end-member microstructure observed in naturally and experimentally deformed rocks (Fig. 4) [15, 16] as follows.

2.2.1. Nucleation and early growth

Structural and/or chemical heterogeneities in the rock are the sites of stress and strain concentration that can induce transient flow instabilities. These primary perturbations include grain and phase boundaries, voids, fluid or solid inclusions, and, in general, structures on all scales that develop before or during shearing. With increasing strain, the instabilities grow into elongated domains oriented subparallel to the shearing plane. Strain-dependent weakening of these domains is usually attibuted to one or a combination of the following processes: rotation of anisotropies [17, 18], dynamic recovery and recrystallization [19], mineral phase transformations [20], strain and strain rate weakening, and fluid weakening [21].

The model at hand disregards the nucleation of instabilities during the initial increments of strain and assumes the existence of a weak phase. At low strains before stage 2 below, the stably deforming part of the rock forms a load-bearing framework (LBF) structure surrounding pockets of unstable weak phase (Fig. 4(a)). The system (strong stable rock plus unstable weak domains) is assumed to deform at or near uniform strain rate, even as the weak instabilities grow at the expense of the framework.

2.2.2. Coalescence and stabilization

After a critical strain, the unstable regions coalesce to form an interconnected weak layer (IWL) structure surrounding elongated lozenges of stronger less

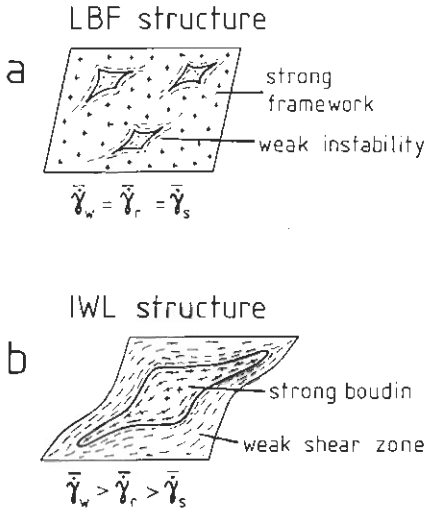

Fig. 4. Ideal structures modelled in this paper: (a) low strain load-bearing framework (LBF) structure; (b) high strain interconnected weak layer (IWL) structure. $\bar{\dot{\gamma}}$ denotes average shear strain rate, and the subscripts r, w and s denote rock, weak phase and strong phase respectively.

deformed rock (Fig. 4(b)). Slip along the incoherent phase boundaries accommodates strain incompatibilities arising from the heterogeneous deformation of the two phases. The growth rate of the interconnected weak instabilities decreases to zero and the IWL structure stabilizes (*i.e.* becomes statistically invariant with time and strain). The attainment of this structural steady state is presumed to coincide with the onset of mechanical steady state (the invariance of bulk flow stress with time and strain). Means [22] refers to such simultaneous structural and mechanical steady state as "true steady state". In the model here, the partitioning of stress and strain rate in a stable IWL structure depends on the strength contrast between the country rock and shear zone, as well as on the stable volume proportions of the phases (see the next section).

Although the deformation of both phases in the LBF and IWL structures is heterogeneous in nature, only the average shear strain rate of each phase is known or specified in the model. Because flow of the hypothetical rock is isochoric and strain compatibility is maintained amongst the constituent phases, the effective (*i.e.* volume-weighted) strain rates of the phases are additive in both LBF and IWL structures:

$$\dot{\gamma}_r = \bar{\dot{\gamma}}_w \phi_w + \bar{\dot{\gamma}}_s \phi_s \tag{1}$$

where $\bar{\dot{\gamma}}_w$ and $\bar{\dot{\gamma}}_s$ are the average shear strain rates of the weak and strong phases respectively, and where ϕ_w and ϕ_s are the volume proportions of weak and strong phases in the rock. The volume of the rock is set equal to unity, so that the volume proportions of the phases sum to unity, $\phi_w + \phi_s = 1$. Note that, because slip is allowed between the phases, this equation implies that the average stress in the two phases can differ. This condition is particularly relevant in the high strain IWL microstructure.

Strain rate is related solely to differential creep stress in the rock because inertial forces are negligible at the low natural strain rates in mylonite (10^{-9}–10^{-15} s^{-1}). For the sake of simplicity and because transient creep in geologic materials is poorly understood [23], the rheology of both phases is assumed to be strain invariant. The empirically derived constitutive equation for creep that relates shear stress τ to average shear strain rate $\bar{\dot{\gamma}}$ in the weak and strong phases is (modified from the expressions of Weertman [24] and Paterson [25])

$$\tau = \exp\left(\frac{1}{n}\left\{\frac{Q}{RT} + \ln\left[\frac{\bar{\dot{\gamma}}\delta^m}{3^{(n+1)/2}A}\right]\right\}\right) \tag{2}$$

where Q is the activation enthalpy of creep, T is the temperature, and δ is the average grain diameter. The exponents n and m are respectively the stress and grain size sensitivities of strain rate. The pre-exponential function A is multiplied by the factor $3^{(n+1)/2}$ [26, 27] to convert the axisymmetric stresses and strain rates of the laboratory flow laws to the plane-strain simple (octahedral) shear configuration assumed here. For the sake of simplicity, both phases are assumed to deform solely by grain-size-insensitive dislocation creep ($m = 0$). The stress value obtained at an average shear strain rate in eqn. (2) slightly overestimates the average stress because minerals undergoing grain-size-insensitive dislocation creep are non-linear (for rock, generally $n = 2$–6 [4]). This discrepancy in stress values increases with decreasing strain rate and increasing values of n, but is small compared with the discrepancies associated with the experimental error in the creep parameters [25].

2.3. Criteria for structural and mechanical steady state in heterogeneous systems

Two questions guide the search for a quantitative criterion of heterogeneous steady state in mylonites: (1) which configuration (LBF or IWL) of weak and strong phases is stabler at given temperature, volume proportions of phases, and bulk strain rate? (2) what are the steady state values of stress, strain rate and volume proportions for the phases in a rock deforming under these same conditions? The first question pertains to structural or configurational steady state, whereas the second question relates primarily to mechanical steady state. A satisfactory criterion of combined structural and mechanical steady state must provide answers to both questions.

To answer the first question it is hypothesized that, for given conditions of deformation, the configuration with the lower rate of total energy dissipation is more stable at the prevailing temperature and bulk strain rate than the configuration with the higher rate of total strain energy dissipation. The total rate of viscous strain energy dissipated in a heterogeneously deforming rock $\dot{E}_r$ is equal to the sum of the volume-weighted rates of energy dissipated in the constituent phases. Another way of stating this is that the power dissipation capacity of a rock is equal to the sum of the power dissipation capacities for each of the phases i in the rock:

$$\dot{E}_r = \sum_{i=1}^{N} \tau_i \dot{\gamma}_i \phi_i \tag{3}$$

where the τ_i and $\dot{\gamma}_i$ are respectively the shear stress and incremental shear strain rate tensors, and the ϕ_i are the volume proportions of the phases. For a two-phase rock, the terms for weak and strong phases are denoted with the subscripts w and s.

In a rock with an ideal low strain LBF structure, the LBF forces the pockets of weak phases to deform at the same average rate as the shear strain rate of the whole rock (Fig. 4(a)). The average power dissipated in a rock with LBF structure $\dot{E}_r^{LBF}$ is found by substituting the uniform strain rate into eqn. (2) for both phases, and then substituting the resultant stress values, together with the uniform strain rate, into the stress and strain rate terms in eqn. (3). Thus

$$\dot{E}_r^{LBF} = \tau_{wr} \dot{\gamma}_r \phi_w + \tau_{sr} \dot{\gamma}_r \phi_s \tag{4}$$

where τ_{wr} and τ_{sr} are the average shear stresses in the weak and strong phases at temperature T and bulk shear strain rate of the rock $\bar{\dot{\gamma}}_r$.

For rock with an ideal high strain IWL structure, the strain rates of the weak and strong phases partition not only according to the volume proportions of those phases in the rock ϕ_w and ϕ_s, but also as a function of the viscous shear strength contrast τ_c, between the phases. τ_c is defined as the ratio τ_{sr}/τ_{wr} of the average octahedral shear stresses in the strong and weak phases measured separately (*i.e.* outside the aggregate) at temperature T and at a reference shear strain rate that equals the overall shear strain rate of the rock $\dot{\gamma}_r$.

Strain rate partitioning in the IWL structure is constrained in the following way.

(a) As the viscous strength contrast of the phases approaches infinity, the bulk strain rate is concentrated into the volume of rock comprising the weak phase, while the average strain rate of the stronger phase tends toward zero. That is $\bar{\dot{\gamma}}_w \to \dot{\gamma}_r \phi_w^{-1}$ and $\bar{\dot{\gamma}}_s \to 0$, where $0 < \phi_w < 1$.

(b) As the viscous strength of the two phases approaches unity (condition of rheological homogeneity), deformation becomes homogeneous and the strain rate in both phases equals that of the rock for any volume proportion of phases: $\bar{\dot{\gamma}}_w = \bar{\dot{\gamma}}_s = \dot{\gamma}_r$ for $0 < \phi_w < 1$.

These two constraints allow an expression to be derived that describes how the average strain rate of the weak phase varies with the strain rate of the rock, and with the volume proportions and the viscous strength contrast of the two phases. This expression is similar to the limit in condition (a) above:

$$\bar{\dot{\gamma}}_w = \dot{\gamma}_r \phi_w^{-x} \tag{5}$$

where x is a function of τ_c for $1 \leqslant \tau_c \leqslant \infty$. The function x is a measure of the τ_c sensitivity of strain rate partitioning in the rock. It determines what proportion of the bulk strain rate is accommodated by the volume of weak phase. Substituting eqn. (5) into eqn. (1) and solving for $\bar{\dot{\gamma}}_s$ yields an expression for the average strain rate of the strong phase:

$$\bar{\dot{\gamma}}_s = \dot{\gamma}_r (1 - \phi_w)^{-1} (1 - \phi_w^{1-x}) \tag{6}$$

The τ_c dependence of x in eqns. (5) and (6) is determined with three constraints: (1) $0 \leqslant x \leqslant 1$ for $0 < \phi_w < 1$ (conditions (a) and (b)); (2) $x \to 1$ as $\tau_c \to \infty$ (condition (a)); (3) $x \to 0$ as $\tau_c \to 1$ (condition (b)). The simplest smooth function that satisfies the constraints on strain rate partitioning at $\tau_c = 1$ and $\tau_c = \infty$ is

$$x = \left(1 - \frac{1}{\tau_c}\right) \qquad 0 < \phi_w < 1 \tag{7}$$

The function x is undefined in rheologically homogeneous rocks, so obviously $\bar{\dot{\gamma}}_w = \dot{\gamma}_r$ at $\phi_w = 1$ and $\bar{\dot{\gamma}}_s = \dot{\gamma}_r$ at $\phi_w = 0$. It is emphasized that the exponential dependence of strain rate partitioning on τ_c derived above is not a unique relation, but merely satisfies the available constraints at the limiting conditions of $\tau_c = 1$ and $\tau_c = \infty$. More complicated relations are conceivable, but not justified in the absence of additional constraints for τ_c values between 1 and ∞.

Equations (5) and (6) are purely phenomenological descriptions of strain rate partitioning in a rock with IWL structure. Nevertheless, when combined with eqn. (7), they facilitate predictions of viscous composite rheology that compare successfully with rheological data for experimentally deformed two-phase aggregates [16].

The average power dissipated in a mylonitic rock with IWL structure is obtained by first substituting eqns. (5) and (6) into eqn. (2), and then substituting the resultant stress values from eqn. (2), together with the strain rates from eqns. (5) and (6), into the stress and strain rate terms in eqn. (3). This yields

$$\dot{E}_r^{IWL} = \dot{\gamma}_r[\tau_w \phi_w^{1-x} + \tau_s (1 - \phi_w^{1-x})] \quad (8)$$

where τ_w and τ_s are the average shear stresses in the weak and strong phases at temperature T, volume proportion ϕ_w and bulk shear strain rate $\dot{\gamma}_r$.

To determine whether the LBF or the IWL structure is stabler at given values of ϕ_w, T and $\dot{\gamma}_r$, one just compares the total power dissipation levels obtained with eqns. (4) and (8) to see which structure dissipates less energy per unit time. Note that this criterion alone suffices to calculate viscous strength *vs.* volume proportion diagrams for any two-phase aggregate in which the volume proportions of the phases is invariant with strain (see the structural stability diagram in Fig. 9 of ref. 16). If the relative amount of phases in the aggregate can vary with strain, however, then an additional criterion is necessary that stipulates a condition of steady state within the heterogeneous system. Without this second criterion, and using only the criterion of power dissipation minimization above, deformation would be predicted to continue until the rock comprised only weak phase and strain is homogeneous.

To answer the second question posed above, therefore, it is postulated that the stress, strain rates and volume proportions of phases remain constant in a rock when the power dissipation capacities of the constituent phases are equal. In other words, heterogeneous steady state in a rock is attained when this rock has a uniform power dissipation capacity. This condition is referred to as internal power equilibrium. For the two-phase rock considered here, the criterion of internal power equilibrium is expressed as

$$\tau_w \dot{\bar{\gamma}}_w \phi_w = \tau_s \dot{\bar{\gamma}}_s \phi_s \quad (9)$$

where all the terms are defined above for the LBF and IWL structures. Equation (9) implies that any viscosity contrast between the constituent phases results in different strain energy dissipation rates, and therefore also in different volume proportions of these phases at dynamic steady state. The steady state values of τ, $\dot{\gamma}_r$ and ϕ for both weak and strong phases can be obtained by solving eqn. (9) iteratively for these terms at constant temperature and bulk shear strain rate.

In summary, the criteria for structural and mechanical steady state proposed above can be combined to form a general criterion for heterogeneous steady state: a rock deforms heterogeneously at steady state when it attains a configuration that minimizes its total power dissipation and when the power dissipation capacity within this structure is uniform and constant.

3. An example: heterogeneous shearing of quartzite

To visualize the concepts outlined above, imagine a mylonitic quartzite comprising two quartz phases with different rheologies. The heterogeneous rheology of this quartzite reflects localized strain-induced variations in its texture, microstructure and defect chemistry (*e.g.* see ref. 5). The criteria postulated in the previous section are used here to calculate the compositional dependence of power dissipation capacity, stress and strain rate in the quartzite and its constituent phases.

The diagrams in Fig. 5 plot normalized power dissipation capacity *vs.* the volume proportion of weak quartz phase, at phase strength contrasts of 2 (Figs. 5(a) and 5(b)) and 5 (Figs. 5(c) and 5(d)). The normalized power dissipation capacity is defined as the power dissipation capacity of a rock or phase divided by the power dissipated in the pure strong phase of that rock (*i.e.* the power dissipated in the strong phase at $\phi_w = 0$ is set equal to unity). Diagrams like this facilitate a direct comparison of the energy dissipation of different sheared materials. The phase strength contrast between the strong and weak quartz phases in Fig. 5 was varied by adjusting the temperature at constant bulk strain rate. The creep parameters were assumed to remain constant throughout the deformation (conditions and experimental creep parameters were as listed in the caption to Fig. 5). However, to simulate the effects of progressive strain on rheology one can also vary τ_c by adjusting the creep parameters of the phases with respect to each other at constant temperature and bulk shear strain rate. Generally, higher values of τ_c correlate with greater bulk shear strain due to the positive feedback relationship between structural and rheological heterogeneity. Strain and time are not incorporated as variables in the equations above used to construct these diagrams, but they both scale with ϕ_w. Therefore the plotted position of a progressively deforming rock in Fig. 5 moves from $\phi_w = 0$ to the right.

The LBF structure is only stable at low volume proportions of weak phase, whereas the IWL structure is stabler over a broad compositional range (Figs. 5(a) and 5(c)). With increasing strength contrast between the phases, the transition from an LBF to an IWL structure shifts to lower values of ϕ_w and therefore also of strain. This structural transition coincides with a jump in the power dissipation capacities of weak and strong phases (Figs. 5(b) and 5(d)). A glance at the relative strain rate and relative stress diagrams in Fig. 6 shows why this is so. In rock with an LBF, the strong phase supports most of the stress and so dissipates much more power per unit volume than do the isolated pockets of weak phase deforming at the same rate. In the IWL structure, however, the contiguous shear zones of weak phase are free to deform much faster than the strong phase and so dissipate strain energy at a greater rate. At high τ_c values, the strain rate partitioning in the IWL structure is so large that the power dissi-

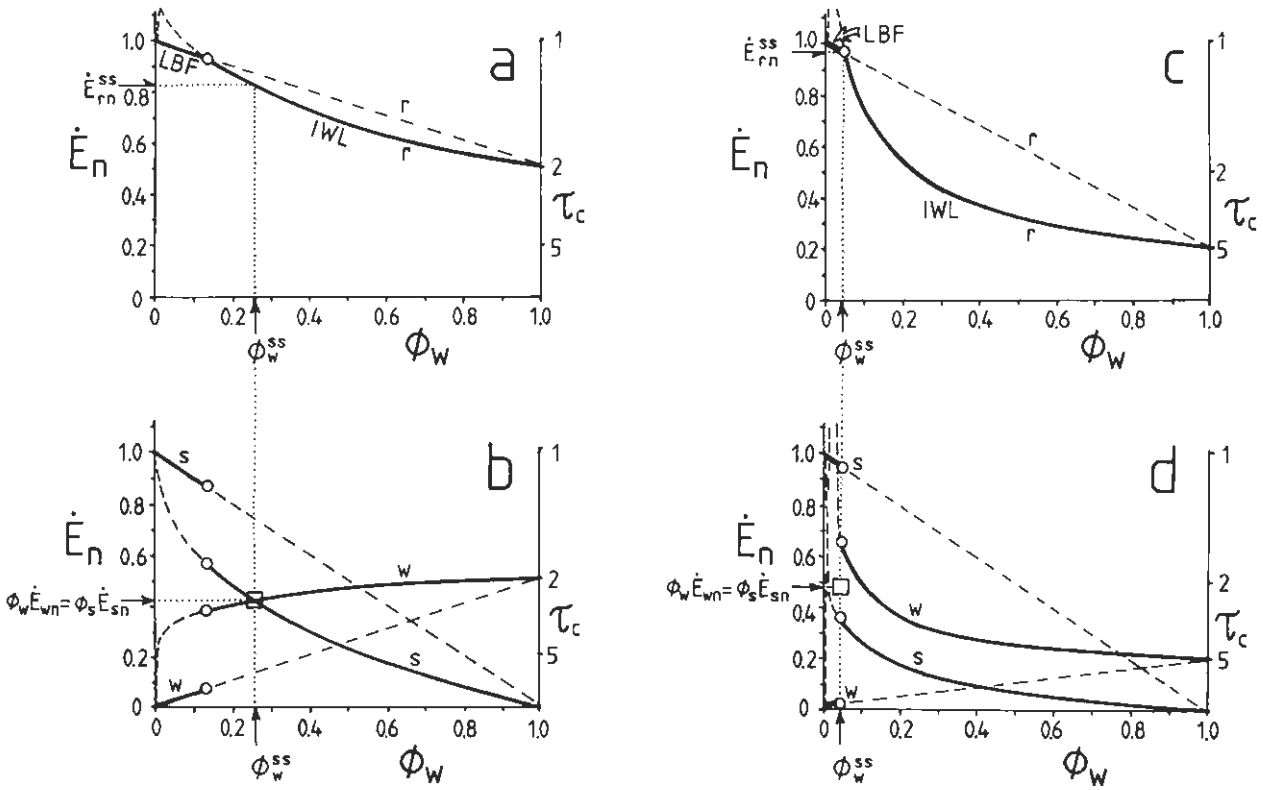

Fig. 5. Plots of normalized power dissipation capacity $\dot{E}_n$ *vs.* volume proportion of weak quartz phase ϕ_w for a heterogeneously deformed quartz mylonite at two values of phase strength contrast τ_c: (a) whole rock at $\tau_c = 2$; (b) phases at $\tau_c = 2$; (c) whole rock at $\tau_c = 5$; (d) phases at $\tau_c = 5$; ——, stable; - - -, metastable; ○, LBF–IWL transition; □, internal power equilibrium. The subscripts r, w, s and ss denote rock, weak phase, strong phase, and steady state values of power dissipation capacity and volume proportion of weak phase (projected orthogonally along thin dotted lines from squares). The steady state creep parameters for quartzite from Jaoul *et al.* [21] were: for weak "water added" Heavitree quartzite $n = 1.4$, $Q = 146$ kJ m^{-1}, $A = 5.25 \times 10^{-3}$ MPa^{-n} s^{-1}; and for strong "as is" Heavitree quartzite $n = 2.4$, $Q = 163$ kJ m^{-1}, $A = 10^{-5}$ MPa^{-n} s^{-1}. The conditions of shearing are constant bulk shear strain rate $\dot{\gamma}_r = 10^{-12}$ s^{-1}, at temperature $T = 240$ °C for $\tau_c = 2$, and $T = 301$ °C for $\tau_c = 5$.

pation capacities of the phases cross at the LBF–IWL transition (Fig. 5(d)). In nature, the power dissipation capacity curves for phases at the LBF–IWL transition are probably not vertical as depicted in Fig. 5, but they certainly may be very steep as strain rate within the LBF structure becomes increasingly non-uniform just before the coalescence of weak instabilities.

The intersection of the stable power dissipation capacity curves in Figs. 5(b) and 5(d) represents the condition of heterogeneous steady state where the power dissipation field in the rock is uniform. This is the point of internal power equilibrium (eqn. (9); squares in Fig. 5). The ϕ_w value beneath this point is the stable volume proportion of active weak shear zones at the ambient temperature and bulk strain rate. Note that the criterion of heterogeneous steady state proposed above in eqn. (9) does not correspond to a minimum in the power dissipation capacity of the whole rock (Figs. 5(a) and 5(c)). Rather, it is the net power dissipation capacity of the phases which is minimized (Figs. 5(b) and 5(d)).

At low values of τ_c, internal power equilibrium occurs within the IWL field, but at higher τ_c values this equilibrium condition coincides with the LBF–IWL transition (Figs. 5(b) and 5(d)). This is seen more clearly in Fig. 7(a), which shows how ϕ_w values at the LBF transition and at internal power equilibrium vary with phase strength contrast. At τ_c values less than 2.8, both ϕ_w values decrease sharply with increased τ_c, and internal power equilibrium occurs in the IWL structural domain. For phase strength contrasts of 2.8 or more, however, internal power equilibrium in this quartz mylonite is inferred to occur at the LBF–IWL transition (stippled parts of curves in Fig. 7(a)). This inference is based on a comparison of the stable and metastable curves in Fig. 5. Their relative positions indicate that internal power equilibrium can never be attained in an LBF structure because this structure is always unstable at ϕ_w values greater than 0.5. Whether a deforming rock reaches internal power equilibrium in the IWL field or at the LBF–IWL transition is expected to depend on the relative rates of localization and rheo-

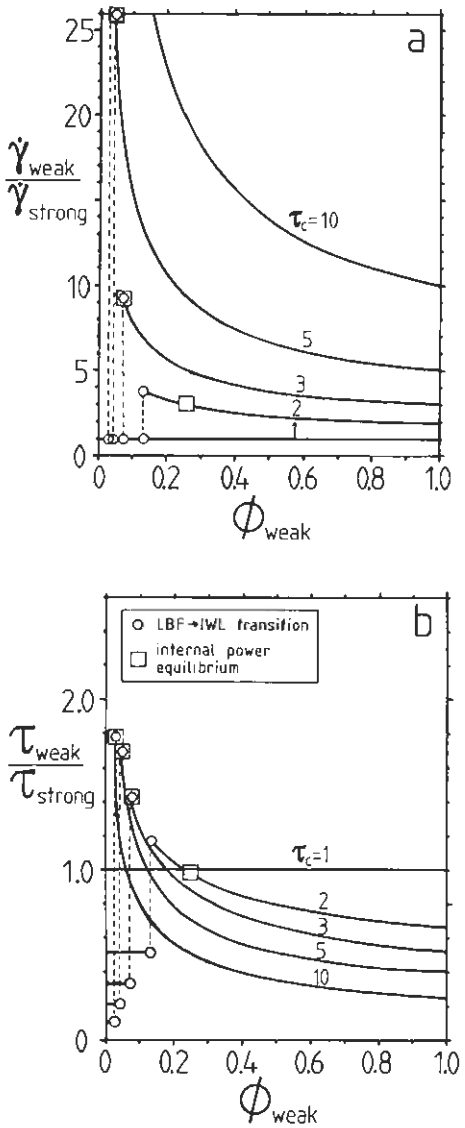

Fig. 6. (a) Relative shear strain rates and (b) relative shear stresses of the weak and strong quartz phases *vs.* volume proportion of weak quartz phase ϕ_w in a quartzite mylonite. ——, Contours for τ_c values from 1 to 10 at a bulk shear strain rate $\dot{\gamma}_t = 10^{-12}\ s^{-1}$; □, internal power equilibrium; ○, transition from LBF (left) to IWL structure (right) in the rock; ⊡, coincidence of internal power equilibrium with the LBF–IWL transition. Creep parameters for quartzite were as in Fig. 5.

logical change. Relatively high rates of localization probably lead to a stable configuration such as that in Figs. 5(a) and 5(b), whereas relatively high rates of rheological change might result in that of Figs. 5(c) and 5(d).

Figure 6 demonstrates that, in quartzite deforming at heterogeneous steady state with moderate to large phase strength contrasts ($\tau_c \geqslant 3$), the shear zones are predicted to deform at higher stress and strain rate than in the country rock. While the strain rate amplification in the shear zones is considerable (Fig. 6(a)), the stress amplification is more modest (Fig. 6(b)). The predicted stress contrasts of up to 2 for strength contrasts of 1–10 (Fig. 6(b)) are within the same order of magnitude as stress amplifications of 1.5–10 estimated from the decrease in dynamically recrystallized quartz grain size across mylonitic shear zones in granitic rocks [28].

Surprisingly perhaps, one finds that straining a rock until it deforms at heterogeneous steady state effects only a modest decrease in its total power dissipation capacity (Figs. 5(a) and 5(c)). For the quartzite considered here, a minimum in the total power dissipation capacity at heterogeneous steady state occurs at a phase strength contrast of about 2 (Fig. 7(b)). This minimum value is still 82% of the power dissipation capacity of the strong quartz phase (Fig. 7(b)). At constant bulk shear strain rate, the normalized power dissipation capacity in the rock is equal to its normalized viscous strength. Thus heterogeneous shearing causes a maximum strength drop of 18% for the quartzite.

4. Discussion

The main point to emerge from the example above is that it is the uniformity of the effective rate of work done within the rock, rather than the minimum absolute rate of work done on the whole rock, which characterizes heterogeneous steady state creep. Although low viscosity shear zones dissipate strain energy at a higher rate (the product of stress and strain rate) than the more viscous country rock, at true steady state they dissipate the same amount of strain energy per unit time (the product of stress, strain rate and volume) as do much larger volumes of more viscous rock deforming at lower strain rates.

Viscous power dissipated in a deformational system at heterogeneous steady state can be regarded as deformational energy that is evenly distributed amongst the phases per increment of time, strain and volume. The net power believed to drive an isothermal viscously deforming system towards heterogeneous steady state can be divided into two components (Fig. 8): (1) a difference in total power dissipation capacity between the LBF and IWL structures; (2) a difference in the power dissipation capacity between the weak and strong phases within these two structures. The LBF–IWL transition is like a spontaneous irreversible reaction that involves a decrease in the overall power dissipation capacity of the rock. Although the total entropy of the rock increases with time and strain, the overall rate of entropy production is inferred to decrease as the phase distribution in the rock becomes progressively less uniform and weak zones interconnect to form a

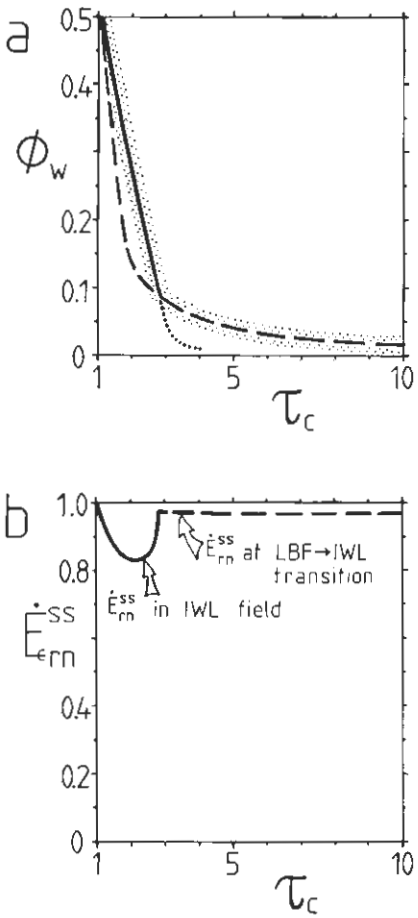

Fig. 7. (a) Volume proportion of weak quartz phase ϕ_w *vs.* phase strength contrast τ_c at the LBF–IWL transition (– – –) and at internal power equilibrium (——): – – –, curve constructed with eqns. (4) and (8); ——, curve constructed with eqn. (9); ···, metastable curve in the LBF field which degenerates at $\tau_c > 3$. Stipples show inferred conditions for heterogeneous steady state (see text). (b) Normalized power dissipation capacity of quartz mylonite at heterogeneous steady state $\dot{E}_{rn}^{ss}$ *vs.* viscous phase contrast τ_c. ——, – – –, curves as in (a). Creep parameters for quartzite are the same as in Figs. 5 and 6.

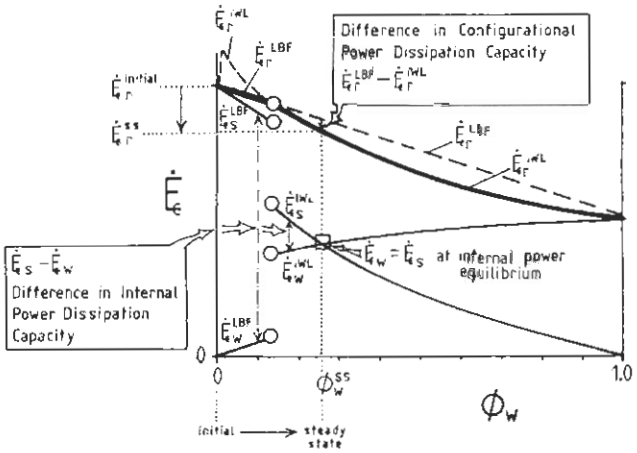

Fig. 8. Schematic plot of power dissipation capacity $\dot{E}$ *vs.* volume proportion of weak phase ϕ_w based on Figs. 5(a) and 5(b). The diagram depicts the net power dissipation capacities associated with (1) the irreversible breakdown of the LBF structure to form an IWL structure, and (2) changes in the volume proportions of weak and strong phases: □, point of internal power equilibrium; ○, LBF-to-IWL transition. The subscripts r, w and s denote whole rock, weak phase and strong phase respectively.

strong anisotropy subparallel to the shearing plane. Once an IWL structure has formed, changes in the power dissipation capacities and volume proportions of the phases are expected to be reversible within the IWL field. Altering the temperature or strain rate will narrow or broaden the shear zones, depending on the phases' relative activation energies and creep exponents. The amounts of strain energy dissipated and entropy produced in a heterogeneous viscous system changing from one structural state to another are path dependent and may be non-linear in time. If so, non-equilibrium thermodynamics might provide the appropriate formalism to describe the energetics of viscously deforming rocks in future studies [29].

This paper has not presented any unequivocal arguments for or against the postulate in eqn. (9) that the power dissipation capacity of a composite is uniform at heterogeneous steady state. Therefore the dilemma of whether to interpret high strain mylonitic shear zones as manifestations of transient rheological instability or of steady state heterogeneous creep remains unresolved. To this author, at least, it seems likely that heterogeneity will always exist on some scale of observation, even though this scale may change with time. If heterogeneous shear is only a transient condition on the path to homogeneous steady state shear, then why do initially homogeneous systems develop instabilities? Research is needed to characterize the link between time and size scales of heterogeneous strain.

The equations of power dissipation partitioning derived above are all hypothetical and clearly require testing. In particular, the strain rate concentration function x in eqns. (5) and (6) is likely to be more complicated than expressed in eqn. (7). Synkinematic microscopy of rock-analogue materials with low melting temperatures (organic compounds [22] and metals [30]) is a promising way of investigating polyphase flow. This method allows the evolution of mylonitic microstructures to be observed under a microscope while the mechanical history of the sample is monitored. Besides more experimental work, the theoretical basis of heterogeneous steady state creep can be extended to account for other processes. For example, synkinematic phase transformations may affect the energy budget of a viscously deforming rock. This is especially

true if such reactions have activation energies comparable with the activation energy of creep and if the reactions occur on the same timescale as the deformation. Deformation mechanisms that involve significant volume change (*e.g.* cataclasis) and/or mass transfer (*e.g.* diffusion creep) amongst the phases also perform work on the system and this can be incorporated into the heterogeneous creep model.

5. Implications for the structural and rheological history of mylonitic shear zones

It is tempting to consider the evolution of mylonitic shear zones in light of the quartzite example and the discussion above. Structural and rheological change during localization can be regarded as the integral of many increments of equilibrium in which material properties vary incrementally with time. This allows the criterion of heterogeneous steady state to be applied to describe how the evolution in energy and stress partitioning within a rock is related to its structure. This is shown qualitatively in Fig. 9 for a hypothetical rock deforming at constant shear strain rate.

Immediately after instabilities nucleate in an initially homogeneous rock, the average stress in the weak unstable pockets is low, even though very high stresses concentrate at their propagating tips. At the same time, stress in the LBF is almost as high as the peak strength of the rock itself. As the framework begins to disintegrate and an IWL structure forms, the strain in the rock becomes progressively less uniform. Power dissipation capacity and creep stress increase sharply in the small volume of coalescing weak phase and drop abruptly in the strong phase. In comparison, the power dissipation capacity and strength of the whole rock falls gradually (Fig. 9).

Once the weak phase coalesces, two end-member histories are envisaged, depending on the rheological contrast of the constituent phases at steady state. In type 1 evolution, if a moderate to high phase contrast is attained (Figs. 9(a) and 9(b)), then stress in the interconnected weak phase reaches a steady state value at the LBF–IWL transition (Fig. 9(b)). This stress is higher than the maximum creep strength of the rock and persists to greater strains because internal power equilibrium coincides with the LBF–IWL transition (Fig. 5(a)). If the creep stress in the strong country rock is less than the mechanism-dependent critical shear

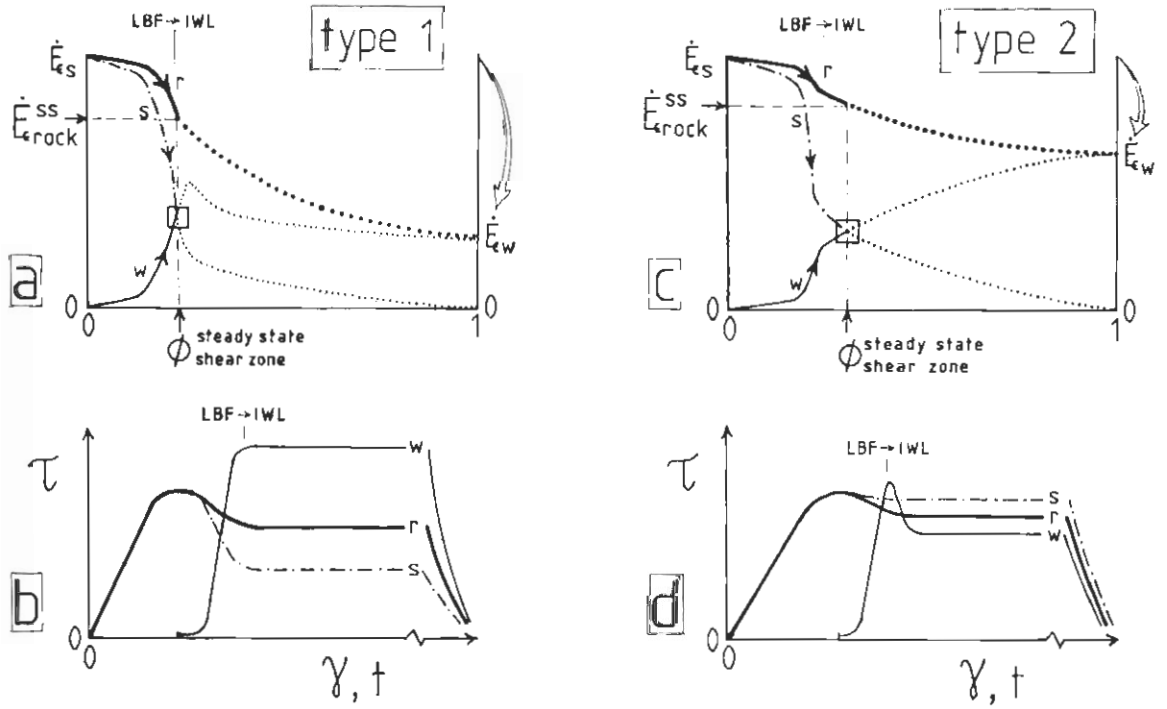

Fig. 9. Evolution of heterogeneously deformed rock described in the text for high steady state τ_c values (type 1) and low to moderate steady state τ_c values (type 2); (a), (c) power dissipation capacity $\dot{E}$ *vs.* volume proportion of weak phase ϕ_w; (b), (d) shear stress τ *vs.* shear strain γ or time t; ⟶, path of deforming rock; – – –, stable curves beyond internal power equilibrium not traversed by deforming rock; □, internal power equilibrium. The superscript ss denotes steady state; the subscripts r, w and s denote whole rock, weak phase and strong phase respectively.

stress required for creep, then the strong phase stops deforming. In type 2 evoluton, for low steady state phase strength contrasts (Figs. 9(c) and 9(d)), creep stress in the weak shear zones relaxes from a peak value at the LBF–IWL transition to a level that is consistent with internal power equilibrium in the IWL field (Fig. 9(d), see also Fig. 5(b)). This postpeak stress drop occurs while the shear zones are still broadening and their power dissipation capacity increases (recall Fig. 5(b)). Unlike type 1 stress histories, the local steady state creep stresses in the shear zone and the country rock are, respectively, less than and greater than the composite stress in the aggregate. Consequently, the country rock continues to creep at a higher stress, albeit at a lower strain rate than the shear zone.

These contrasting mechanical histories are expected to leave different microstructural signatures in rock. During a type 2 history, continued creep in the country rock after localization overprints older structures. In rocks with a type 1 history, however, the microstructures associated with deformation before localization are preserved outside the shear zones if the following two conditions are met. (1) The stress drop adjacent to the narrowing shear zones is fast compared with the stress sensitivity of the microstructures. Prior *et al.* [31] estimate minimum stress relaxation rates of about 10^{-9}–10^{-11} MPa s^{-1} for the preservation of dynamically recrystallized quartz grains in greenschist facies mylonites ($T \approx 350$ °C, $P \approx 300$ MPa). (2) The ambient temperature is sufficiently low, or the cooling time is fast enough, to inhibit static recrystallization and annealing. The kinetics of static grain growth in quartz become very sluggish at temperatures below about 300 °C [32]. Stress histories other than those shown in Fig. 9 are possible, depending on the combination of creep parameters and physical conditions used in eqns. (4)–(9). However, a complete analysis of these mechanical histories and their geological implications lies beyond the scope of this paper and will be treated elsewhere.

The concepts of power partitioning expressed in eqns. (5)–(9) provide a plausible explanation for the common observation in mylonitic shear zones of grain size reduction involving dynamic recovery and *in situ* dynamic recrystallization (*e.g.* Bell and Etheridge [33]). In this type of dynamic recrystallization, the strain-dependent polygonization of subgrains leads to the nucleation of new strain-free grains which then grow at the expense of larger, older, strained grains (*e.g.* see ref. 34, and the regime 2 dynamic recrystallization of Hirth and Tullis [35]). The high rate of strain energy dissipated in shear zones leads to a local increase in the average unbound dislocation density and so augments the stored crystal plastic energy. This energy drives dynamic recovery and recrystallization, and the nucleation rate of new small grains increases with respect to the rate of grain growth. The average grain size in shear zone then decreases for two reasons: (1) the proportion of new, strain-free, grains increases with increasing strain [35, 36]; (2) the grain size in dynamic equilibrium with creep stress in the shear zone [37, 38] is often smaller than the size of the old (usually statically recrystallized) grains in the country rock. Note that the occurrence of small dynamically recrystallized grains in shear zones does not necessarily mean that the creep stress in the shear zone was higher than in the country rock, but merely that the product of stress and strain rate in the shear zone was higher. However, if subgrains and dynamically recrystallized grain sizes decrease across a shear zone or shear band [39] and these grains can be shown to have formed simultaneously (*e.g.* Fig. 1(d) above, and Figs. 2–4 in ref. 16), then it is possible to infer a stress concentration in the shear zone (type 1 evolution in Fig. 9(b)). Microstructural gradients across shear zones are preserved at the end of the deformation if the stress decreases abruptly in the whole rock, effectively freezing in the microstructure in all parts of the rock simultaneously.

6. Conclusions

Mylonitic rock may deform heterogeneously at steady state if it attains a structure that minimizes its total power dissipation and if the power dissipation capacity within this structure is uniform and constant. The strain-dependent growth and coalescence of rheological instabilities to form interconnected shear zones is believed to be an irreversible process that effects only a modest reduction in total rock strength, but that leads to significant changes in stress and strain rate partitioning between the constituent phases. Therefore the strength evolution of a heterogeneous rock differs significantly from its internal stress history.

To the extent that they predict heterogeneous behaviour in rocks, the steady state criteria proposed in this paper may apply to all viscous composite substances. There are potential applications of this work in both the geological and materials engineering sciences. For example, the mixed phase flow laws in eqns. (4) and (8) enable geologists to estimate the dependence of lithospheric strength on rock composition [16] and strain heterogeneity. Such information may be useful in refining mechanistic models of seismicity. The criteria of heterogeneous steady state in this paper were developed with an awareness that understanding steady state is the first simple step towards a more sophisticated treatment of polyphase viscous media such as mylonitic rocks.

Acknowledgments

First, I would like to thank Ruedi Wenk, Kristin Bennett and Dawn Janney for organizing this most interesting meeting. In Palm Springs, I benefited from many discussions with other participants, especially L. Anand, P. Bons, Y. Brechet and J. Tullis. The reviews of Jan Tullis and Ruedi Wenk, and written correspondence with Yves Bréchet and Win Means, led to several improvements in the formulation of ideas in this paper. Prior to the meeting, I enjoyed stimulating debates on polyphase flow with Renée Heilbronner-Panozzo, Marco Herwegh, Stefan Schmid and Holger Stuenitz. All of the above are thanked for their time and interest. This research, and the travel costs to attend the conference, were financed by a Profil-2 grant from the Swiss National Science Foundation (Project 21-30598.91).

References

1 M. R. Handy and A. Zingg, *Geol. Soc. Am. Bull., 103* (1991) 236–253.
2 P. R. Cobbold, *Can. J. Earth Sci., 14* (1977) 1721–1731.
3 P. R. Cobbold, *Can. J. Earth Sci., 14* (1977) 2510–2523.
4 N. L. Carter and M. C. Tsenn, *Tectonophysics, 136* (1987) 27–63.
5 S. H. White, S. E. Burrows, J. Carreras, N. D. Shaw and F. J. Humphreys, *J. Struct. Geol., 2* (1–2) (1980) 175–187.
6 J. Tullis, A. W. Snoke and V. R. Todd, *Geology, 10* (1982) 227–230.
7 R. J. Knipe, *J. Struct. Geol., 11* (1–2) (1989) 127–146.
8 S. M. Schmid and M. R. Handy, in D. M. Müller, J. A. McKenzie and H. Weissert (eds.), *Controversies in Modern Geology*, Academic Press, London, 1991, pp. 339–362.
9 J. G. Ramsay, *J. Struct. Geol., 2* (1980) 83–99.
10 J. G. Ramsay and M. I. Huber, *The Techniques of Modern Structural Geology*, Vol. 2, *Folds and Fractures*, Academic Press, London, 1987, pp. 595–638.
11 J. G. Ramsay and R. H. Graham, *Can. J. Earth Sci., 7* (1970) 786–813.
12 J. Grocott and J. Watterson, *J. Struct. Geol., 2* (1–2) (1980) 111–117.
13 S. H. Kirby, *Tectonophysics, 119* (1985) 1–27.
14 M. R. Handy, *Tectonophysics, 163* (1989) 119–152.
15 M. R. Handy, *J. Geophys. Res. B, 95* (6) (1990) 8647–8661.
16 M. R. Handy, *J. Struct. Geol.*, in press.
17 P. R. Cobbold and D. Gapais, *Tectonophysics, 131* (1986) 113–132.
18 D. Gapais and P. R. Cobbold, *Tectonophysics, 138* (1987) 289–309.
19 D. H. Zeuch, *Tectonophysics, 83* (1982) 293–308.
20 K. H. Brodie and E. H. Rutter, *Adv. Phys. Chem., 4* (1985) 138–179.
21 O. Jaoul, J. Tullis and A. Kronenberg, *J. Geophys. Res., 89* (1984) 4298–4312.
22 W. D. Means, *Tectonophysics, 78* (1981) 179–199.
23 N. L. Carter and S. H. Kirby, *Pure Appl. Geophys., 116* (1978) 807–839.
24 J. Weertman, *Trans. Am. Soc. Met., 61* (1968) 681–694.
25 M. S. Paterson, *Tectonophysics, 133* (1987) 33–43.
26 J. F. Nye, *Proc. R. Soc. London, 219* (1953) 477–489.
27 R. L. Stocker and M. F. Ashby, *Rev. Geophys. Space Phys., 11* (1973) 391–426.
28 S. H. White, *J. Geol. Soc. London, 131* (1975) 577–583.
29 J. S. Kirkaldy, *Rep. Prog. Phys., 55* (1992) 723–795.
30 S. H. White, M. R. Drury, S. E. Ion and F. J. Humphreys, *Phys. Earth Planetary Interiors, 40* (1985) 201–207.
31 D. J. Prior, R. J. Knipe and M. R. Handy, in R. J. Knipe and E. H. Rutter (eds.), *Deformation Mechanisms, Rheology and Tectonics, Special Publication 54*, Geological Society, London, 1990, pp. 309–320.
32 R. Joesten, *Am. J. Sci. A, 238* (1983) 233–254.
33 T. H. Bell and M. A. Etheridge, *Lithos, 6* (1973) 337–348.
34 S. H. White, *Philos. Trans. R. Soc. London, Ser. A, 283* (1976) 69–86.
35 G. Hirth and J. Tullis, *J. Struct. Geol., 14* (1992) 145–160.
36 M. A. Etheridge and J. C. Wilkie, *Tectonophysics, 78* (1981) 471–492.
37 R. J. Twiss, *Pure Appl. Geophys., 115* (1977) 227–244.
38 G. H. Edward, M. A. Etheridge and B. E. Hobbs, *Textures Microstruct., 5* (1982) 127–152.
39 S. H. White, *Contrib. Mineral. Petrol., 70* (1979) 193–202.